Available online at www.sciencedirect.com
SCIENCE DIRECT®
C. R. Mecanique 333 (2005) 676–682
COMPTES RENDUS MECANIQUE
http://france.elsevier.com/direct/CRAS2B/

Computational AeroAcoustics: from acoustic sources modeling to farfield radiated noise prediction

Computational aeroacoustics applications based on a discontinuous Galerkin method

Philippe Delorme [a,*], Pierre Mazet [b], Christophe Peyret [a], Yoan Ventribout [b]

[a] *ONERA/DSNA, BP 72, 92322 Châtillon cedex, France*
[b] *ONECERT/DTIM, BP 4025, 31055 Toulouse cedex, France*

Available online 9 September 2005

Abstract

CAA simulation requires the calculation of the propagation of acoustic waves with low numerical dissipation and dispersion error, and to take into account complex geometries. To give, at the same time, an answer to both challenges, a Discontinuous Galerkin Method is developed for Computational AeroAcoustics. Euler's linearized equations are solved with the Discontinuous Galerkin Method using flux splitting technics. Boundary conditions are established for rigid wall, non-reflective boundary and imposed values. A first validation, for induct propagation is realized. Then, applications illustrate: the Chu and Kovasznay's decomposition of perturbation inside uniform flow in term of independent acoustic and rotational modes, Kelvin–Helmholtz instability and acoustic diffraction by an air wing. ***To cite this article: Ph. Delorme et al., C. R. Mecanique 333 (2005).***

Résumé

Applications de l'aéroacoustique numérique basées sur une méthode de Galerkine discontinue. La simulation de la propagation aéroacoustique impose de calculer la propagation d'une onde acoustique dans un écoulement inhomogène, avec une faible erreur numérique de dissipation et de dispersion, tout en prenant en compte des géométries complexes. Pour tenter de donner, une réponse trés générale, une méthode de Galerkine discontinue du premier ordre a été mise en œuvre pour l'aéroacoustique numérique. Les équations d'Euler linéarisées sont résolues avec la méthode de Galerkin discontinue, en utilisant la technique dite du *flux splitting*. Des conditions aux limites sont établies pour des parois rigides, des parois traitées, une condition de non-réflexion et des valeurs imposées. Une première validation est réalisée dans le cadre de la propagation en conduit de longueur infinie. Puis, des applications variées illustrent le potentiel de la méthode : décomposition de Chu et de Kovaznay d'une perturbation à l'intérieur d'un écoulement uniforme en modes acoustiques et de rotation, instabilité de Kelvin–Helmholtz et diffraction acoustique par une aile d'avion. ***Pour citer cet article : Ph. Delorme et al., C. R. Mecanique 333 (2005).***

Keywords: Acoustics; Discontinuous Galerkin method; Computational aeroacoustics

Mots-clés : Acoustique ; Méthode de Galerkine discontinue ; Aéroacoustique numérique

* Corresponding author.
E-mail addresses: delorme@onera.fr (Ph. Delorme), mazet@onecert.fr (P. Mazet), peyret@onera.fr (C. Peyret), ventribout@onecert.fr (Y. Ventribout).

1631-0721/$ – see front matter
doi:10.1016/j.crme.2005.07.007

1. Introduction

CAA involves two main problems at the same time. First, the numerical method must be able to simulate acoustic wave propagation with low numerical dissipation and low numerical dispersion. Second, it requires to take into account real geometries. The high-order FDM (Finite Difference Method) schemes, initially introduced by Tam [1], are a good answer to the first problem but, the simulation of acoustic scattering by realistic geometries still remains problematic because, the structured meshing of real geometries is often complex. The Finite Element Method uses unstructured meshes but, it is still not able to solve Euler's linearized equation without spurious mode. Recent improvement of computing technology make today accessible the Discontinuous Galerkin Method for CAA [2]. The method is a quite relevant external approximation. It simulates wave propagation with a small level of dissipation, without dispersion and allows to use automatic mesh maker or mesh refinement technics [3].

2. Physical model

Euler's linearized equations are computed. Assuming a subsonic flow, the entropy equation is used (rather than the energy equation). Supposing at initial time, entropy is spatially uniform, it remains spatially uniform at any time. Such an hypothesis is not essential for the method but, it is commonly done and provides a smaller sized problem. The partial differential equations system is a Friedrich's system due to the Godonov–Mock's theorem asserting the system is symmetric if and only if a *mathematical entropy* exists. Concerning our problem, using variable $\vec{\varphi} = (u_1, v_1, a_0\rho_1/\rho_0)$[1], it results in the symmetric system:

$$\partial_t \vec{\varphi} + \mathcal{A}_i \partial_i \vec{\varphi} + \mathcal{B}\vec{\varphi} = \vec{0}$$

where:

$$\mathcal{A}_1 = \begin{bmatrix} u_0 & 0 & a_0 \\ 0 & u_0 & 0 \\ a_0 & 0 & u_0 \end{bmatrix}, \quad \mathcal{A}_2 = \begin{bmatrix} v_0 & 0 & 0 \\ 0 & v_0 & a_0 \\ 0 & a_0 & v_0 \end{bmatrix}, \quad \mathcal{B} = \begin{bmatrix} \partial_x u_0 & \partial_y u_0 & -\partial_x a_0 \\ \partial_x v_0 & \partial_y v_0 & -\partial_y a_0 \\ \frac{a_0}{\rho_0}\partial_x \rho_0 & \frac{a_0}{\rho_0}\partial_y \rho_0 & (\gamma - 1)\,(\partial_x u_0 + \partial_y v_0) \end{bmatrix}$$

As matrix $\mathcal{A}_i \partial_i$ is symmetric, matrix $\mathcal{A}_i n_i$ is diagonalizable; this is an important remark for the method presented in this paper. Moreover, we are able to write the *mathematical energy* balance:

$$\partial_t \int_{\Omega} \frac{1}{2}\,\vec{\varphi}^2 + \frac{1}{2} \oint_{\partial\Omega} \vec{\varphi}^t \mathcal{A}^i n_i \vec{\varphi} + \frac{1}{2} \int_{\Omega} \vec{\varphi}^t \big(\mathcal{B} + \mathcal{B}^t - \partial_i \mathcal{A}^i\big)\vec{\varphi} = 0 \tag{1}$$

This *mathematical energy* balance has a physical sense. Indeed, it is the sum per mass unit of kinetic energy $(u_1^2 + v_1^2)/2$ and acoustic energy $a_0^2\rho_1^2/\rho_0^2$. In (1), the second term is obviously the flux and the third term is the source of this energy. Matrix $\mathcal{B} + \mathcal{B}^t - \partial_i \mathcal{A}_i$ vanishes when flow is uniform. Otherwise, the matrix does not have a determined sign. It means energy can increase indefinitely depending on the flow stability.

3. Discontinuous Galerkin method

Only main features of the method are presented in this Note and for more details we invite one to read Refs. [4,5].

[1] Where (u_1, v_1) is the acoustic velocity vector, ρ_1 the acoustic density, a_0 the sound speed and ρ_0 the mean flow density.

3.1. Variational formulation

For a k-order DGM, test and interpolation functions are chosen in same functional space composed by the set $\{W^k, k \in N\}$ of kth order polynomials inside each element. It may be discontinuous on edges bordering elements so, the functional space is piecewise W^k polynomial functions. The fact that both, test and interpolation functions are discontinuous prevent from directly writing a weak formulation for all domains. Actually, the DGM is a patchwork of weak formulations inside each element and boundary conditions are connecting elements to each other. For local element ω_h, the weak formulation can be expressed:

$$\forall h,\ \forall \vec{\psi}_h \in W^k(\omega_h), \quad \int_{\omega_h} \left(\partial_t \vec{\varphi}_h + \mathcal{A}_i \partial_i \vec{\varphi}_h + \mathcal{B}\vec{\varphi}_h\right) \cdot \vec{\psi}_h + \oint_{\partial\omega_h} \mathcal{M}(n)\left(\vec{\varphi}_h^o - \vec{\varphi}_h^i\right) \cdot \vec{\psi}_h^i = \int_{\omega_h} \vec{g} \cdot \vec{\psi}_h \tag{2}$$

where $\vec{\varphi}^o$ means the exterior trace, $\vec{\varphi}^i$ the interior one and $\vec{g}$ is the source. $\mathcal{M}$ is a boundary operator. By summation on h:

$$\mathcal{L}(\vec{\varphi}_h, \vec{\psi}_h) = \int_{\Omega} \left(\partial_t \vec{\varphi}_h + A_i \partial_i \vec{\varphi}_h + B\vec{\varphi}_h\right) \cdot \vec{\psi}_h + \sum_h \oint_{\partial\omega_h} \mathcal{M}(n)\left(\vec{\varphi}_h^o - \vec{\varphi}_h^i\right) \cdot \vec{\psi}_h^i - \int_{\Omega} \vec{g} \cdot \vec{\psi}_h = 0 \tag{3}$$

The first term and the third term are usually the same for the all DGM (up to a summation by parts), but the second one depends on the method. The method we have chosen is called characteristics method because it generalizes the characteristics method in 1D. As $A_i n_i$ is symmetric, this matrix is diagonalizable and can be splitted into a positive (set of positive eigenvalues) and a negative part (set of negative eigenvalues):

$$\mathcal{A}_i n_i = [\mathcal{A}_i n_i]^+ + [\mathcal{A}_i \cdot n_i]^-$$

In this method $\mathcal{M} = [\mathcal{A}_i \cdot n_i]^-$, it is a fully upwind scheme. If using kth order polynomials, the precision order is $k+1$.

3.2. Solver

When harmonic solution exists without absolute instabilities in the Huerre and Monkewitz's sense [6], an harmonic solver is used to compute the solution. Otherwise, a time solver based on a second-order Runge–Kutta method is used, in that case, a CFL condition must be satisfied [7].

3.3. Boundary conditions

Consider the element ω_j localized in contact with border $\partial\Omega$. We have $\partial\omega_j \cap \partial\Omega \neq \emptyset$ and boundary conditions are imposed on the segment of ω_j in contact with $\partial\Omega$ (a_1, for example). In local representation, the variational formulation can be written:

$$\begin{aligned}\int_{\omega_j} {}^t\vec{\psi}\mathcal{I}\left(\partial_t\vec{\varphi} + \mathcal{A}_i\partial_i\vec{\varphi} + \mathcal{B}\vec{\varphi}\right) + \oint_{a_1} {}^t\vec{\psi}_{[d_2,d_3]}\mathcal{M}\vec{\varphi}_{[d_2,d_3]} - \oint_{a_1} {}^t\vec{\psi}_{[d_2,d_3]}\mathcal{I}\vec{g} \\ + \oint_{a_2} {}^t\vec{\psi}_{[d_3,d_1]}[\mathcal{A}_i n_i]^-\left(\vec{\varphi}_{[d_6,d_7]} - \vec{\varphi}_{[d_3,d_1]}\right) + \oint_{a_3} {}^t\vec{\psi}_{[d_1,d_2]}[\mathcal{A}_i\, n_i]^-\left(\vec{\varphi}_{[d_8,d_9]} - \vec{\varphi}_{[d_1,d_2]}\right)\end{aligned}$$

Boundary conditions are introduced in the variational formulation with specific expressions of $\mathcal{M}$ and $\vec{g}$:

– for rigid or lined walls ($p_1 = Z\vec{v}_1 \cdot \vec{n}$), where Z is the impedance, and we find:

$$\mathcal{M}(\beta) = \frac{a_0}{2}\begin{bmatrix} (1+\beta)\,\vec{n}\otimes\vec{n} & (\beta-1)\vec{n} \\ -(1+\beta)\,{}^t\vec{n} & (1-\beta) \end{bmatrix} \quad \text{where } \beta = \frac{Z-1}{Z+1} \text{ is the transmission coefficient}$$

$\mathcal{M}(\beta)$ formulation leads to a β-independent CFL condition [7] which is not true for $\mathcal{M}(Z)$ formulation, this property is important for inverse problem. If $\beta = 1$, the walls are rigid (hard sound obstacle). If $\beta = 0$, this is a plane wave impedance, used as an imperfect (1st order) non-reflective boundary condition.

– for imposed value condition

$$\mathcal{M} = -[\mathcal{A}^i n_i]^- \quad \text{and} \quad \vec{g} = \vec{\varphi}_0$$

Those expressions lead to a well-posed mathematical problem in the temporal case [7].

4. Induct propagation

Elements P_0 to P_6 have been implemented and are used to approximate acoustics while a P_1 approximation is used for flow fluid variables ($\vec{v}_0$, p_0, ρ_0). We are studying the precision of the DGM depending on the mesh refinement. Consider an infinite linear duct whose constant cross section is $1/2$ meter, the duct contains air. Domain Ω is shown in Fig. 1, it is a 3 m long portion of the duct. To simulate propagation in an infinite duct, modal solution $n = 0$ at frequency $f = 3.4$ kHz is imposed at the portion entrance (left) and non-reflexion boundary conditions at the exit (right). The walls of the duct are rigid (up and down). For mode $n = 0$ and only for this mode, our 'imperfect non-reflexion boundary conditions' works perfectly.

To compare analytic and computed solutions, a cut along axis ($y = 0.25$ m) is realized and acoustic pressure is plotted on a 2D-plot. At $f = 3.4$ kHz, the number of wavelengths for a 3 m long portion is 30. Comparisons are presented for P_1 in Figs. 2 and 3. The analytical solution whose expression is:

$$p_1(x, y, t) = \sin\left(2\pi f t - \frac{2\pi}{\lambda} x\right)$$

is the paler plot and computed solution is in black.

This results shows for P_1 elements a minimal $\lambda/12$ mesh discretization is required to avoid important numerical dissipation and to keep a good agreement with the analytical solution. Similar computations have been handle for elements P_0 to P_6 and minimal mesh refinement requirements are listed in Table 1. This results are in good agreement with 1D analysis [8]. Note in any case, the dispersion error is low due to the fully upwind scheme.

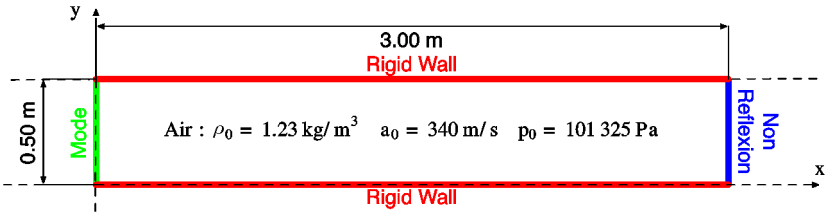

Fig. 1. Domain Ω.

Fig. 1. Domaine Ω.

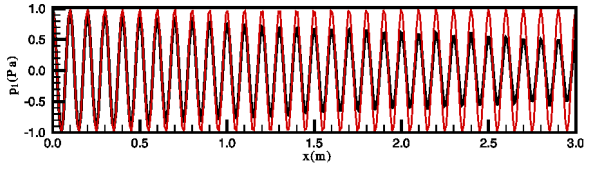

Fig. 2. $p_1(x, 0.25)$ (Pa) – Rigid Walls – mesh $\lambda/7$.

Fig. 2. $p_1(x, 0.25)$ (Pa) – parois rigides – maillage $\lambda/7$.

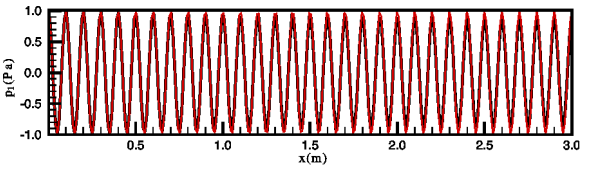

Fig. 3. $p_1(x, 0.25)$ (Pa) – Rigid Walls – mesh $\lambda/12$.

Fig. 3. $p_1(x, 0.25)$ (Pa) – parois rigides – maillage $\lambda/12$.

Table 1
Element order versus mesh refinement

Tableau 1
Ordre de l'élément suivant la discrétisation

P_j	0	1	2	3	4	5	6
h	$\frac{\lambda}{40}$	$\frac{\lambda}{14}$	$\frac{\lambda}{4}$	$\frac{\lambda}{3}$	$\frac{\lambda}{2}$	$\frac{\lambda}{2}$	λ

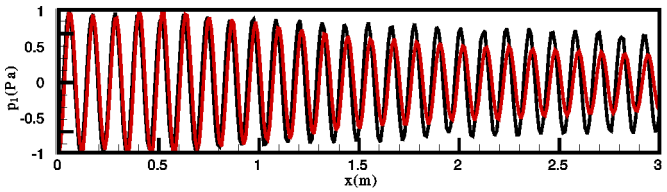

Fig. 4. $p_1(x, 0.25)$ (Pa) – Lined Walls – mesh $\lambda/12$.
Fig. 4. $p_1(x, 0.25)$ (Pa) – parois traitées – maillage $\lambda/12$.

The analytical solution for modes propagating inside an infinite linear lined duct in the presence of a shear flow is found solving Lilley's equation [9,10]. We are going to compare the analytical solution to the DGM computed solution. Consider air contained inside the domain presented in Fig. 1 is moving with celerity:

$$v_0 = \begin{cases} 50\tanh(15y) & \text{if } y \leqslant 0.25 \text{ m} \\ 50\tanh(15(0.5-y)) & \text{if } y > 0.25 \text{ m} \end{cases} \quad \text{(m/s)}$$

Analytical and computed solutions are plotted in Fig. 4 with same representation as previously and are found to be in good agreement when mesh discretization is about $\lambda/12$.

5. Acoustic and rotational modes and Kelvin–Helmholtz instability

In 1958, Chu and Kovasznay [11] initiated the decomposition of perturbations inside uniform flow in terms of independent acoustic, rotational and entropic modes. For isentropic transformation, entropic modes do not exist. The DGM is based on Euler's linearized equations. If we introduce a source containing acoustic and rotational modes in the presence of a uniform flow, simulations should be able to point out the propagation of these two different modes. Inside domain Ω flow is uniform: $\vec{v}_0$ (m/s) $= 100\vec{x}$. Non-reflective boundary conditions are imposed on $\partial\Omega$. On the element containing point $(0.50, 0.25)$, we introduce a source that $\vec{\nabla}\times\vec{v}_1 \neq \vec{0}$ and $\vec{\nabla}\cdot\vec{v}_1 \neq 0$. A numerical simulation based on the DGM is realized. In Fig. 5, the acoustic pressure field is plotted and shows two different modes propagating with different speeds. A deeper analysis of results shows a good agreement with the Chu and Kovasznay's prognostication. There is a flow convected rotational mode and an acoustic mode propagation. Computation was stopped before rotational mode reached the non-reflective border. The boundary condition used to simulation a no-reflection does not work for rotational mode.

Inside a non-uniform flow, the decomposition initiated by Chu and Kovasznay is no longer valid, because of the flow gradients exchanges between flow and aeroacoustics. Consider the configuration of previous section where the flow profile versus y has tanh variations with an inflection on line $(y = 0.25)$ (shear layer). On the inflection line $(y = 0.25)$, flow speed is $v_0 = 100$ m/s. A simulation based on the DGM is realized. The computed values for acoustic pressure are plotted in Fig. 6. The simulation clearly shows an instability slowly developing. and moving with speed $v_0 = 100$ m/s. Again, the computation was stopped before the instability reaches the non-reflective boundary condition because the conditions used are not suitable for instabilities, PML technics under development should solve that difficulty.

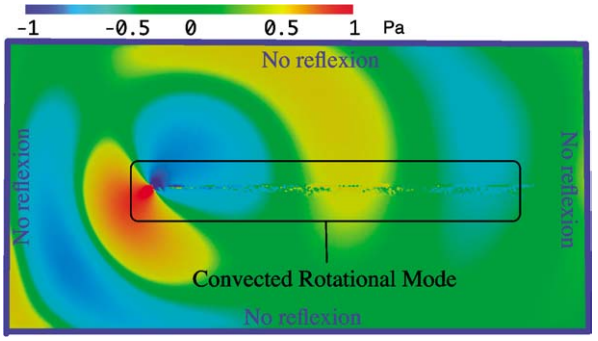

Fig. 5. Acoustic and Rotational Modes, p_1.

Fig. 5. Modes acoustiques et rotationnelle, p_1.

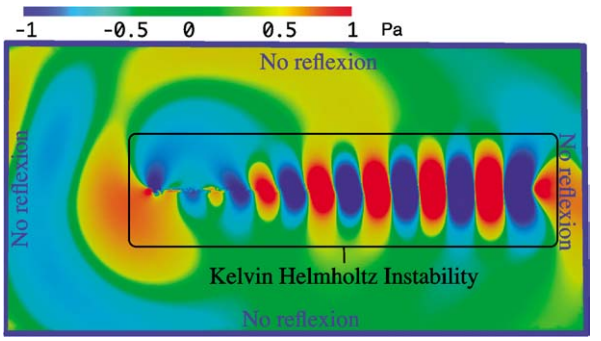

Fig. 6. Kelvin–Helmholtz instability, p_1.

Fig. 6. Instabilité de Kelvin–Helmholtz, p_1.

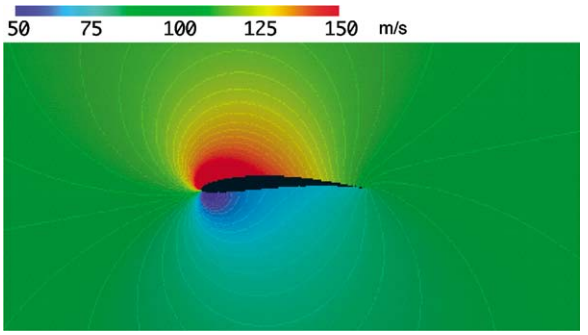

Fig. 7. Flow speed v_0.

Fig. 7. Vitesse de l'écoulement.

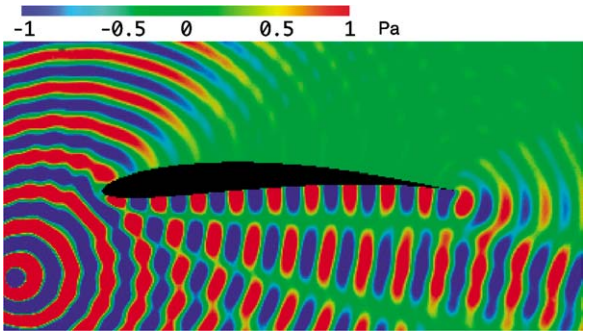

Fig. 8. $f = 2$ kHz, Acoustic pressure field p_1.

Fig. 8. 2 kHz, champ de pression acoustique p_1.

6. Acoustic diffraction

The computation of acoustic diffraction is important for environmental impact and to study the noise generated by airplanes at take-off. We are going to study the acoustic diffraction of noise by a Joukovsky air wing profile. A 2D domain containing the profile is meshed. Non-reflective boundary conditions are imposed on the domain's border and rigid wall boundary conditions are imposed around the profile. Joukovsky profile is chosen because it prevents from complementary CFD computations as the flow speed is given with analytical expressions. The flow speed is irrotational $\vec{\nabla} \times \vec{v}_0 \neq \vec{0}$ and such computations could be carry on with potential equation. However, the DGM remains more general and is able to carry on acoustic diffraction computations for different profiles and to use Euler's or Navier Stockes equations based CFD computations. Numerical values of v_0 are plotted in Fig. 7.

An harmonic monopole acoustic source pulsing at $f = 2$ kHz is placed at point $(-1.5, -0.5)$. A simulation is realized and the acoustic pressure corresponding to the computed solution is plotted in Fig. 8. The figure clearly shows the acoustic diffraction resulting from the presence of the air wing.

7. Conclusion

The Discontinuous Galerkin Method presents many advantages to solve Euler's linearized equations system for studying Computational AeroAcoustics problems. Complex geometries are easily introduced using automatic mesh maker programs. Because of its mathematical foundations, the method is accurate, robust and suitable for complex

industrial problems. The CPU and memory requirement are the main disadvantages and they are less important for high order numerical schemes. The results presented in the paper, show the flexibility and quality of the method for computational aeroacoustics.

References

[1] C.W. Tam, J.C. Webb, Dispersion-relation-preserving finite difference schemes for computational acoustics, J. Comput. Phys. 107 (1993) 262–281.
[2] D.P. Lockard, H.L. Atkins, Efficient implementations of the quadrature-free discontinuous Galerkin method, AIAA J. (1999) 1–11, paper 99-3309.
[3] P. Frey, P.-L. George, Maillages applications aux éléments finis, Hermes, Paris, 1999.
[4] F. Bourdel, J.-P. Croisille, Ph. Delorme, P.-A. Mazet, Sur l'approximation par éléments finis des systèmes hyperboliques k-diagonalisables. Applications aux équations d'Euler et aux mélanges de gaz, Recherche Aérospatiale 5 (septembre–octobre) (1989) 15–34.
[5] F. Bourdel, P.-A. Mazet, Ph. Helluy, Resolution of the non-stationary or harmonic Maxwell equations by a discontinuous finite element method. application to an electromagnetic impulse case, Comput. Methods Appl. Sci. Engrg. (1992) 405–422.
[6] P. Huerre, P.A. Monkewitz, Absolute and convective instabilities in free shear layers, J. Fluid Mech. 159 (1985) 151–168.
[7] Y. Ventribout and P.-A. Mazet, Contrôle d'onde acoustique par impédance de paroi, in: Congrès d'Analyse Numérique, Canum, 2003.
[8] F.Q. Hu, H.L. Atkins, Eigensolution analysis of the discontinuous Galerkin method with nonuniform grids I. One space dimension, J. Comput. Phys. 182 (2) (2002) 516–545.
[9] G. Lilley, Theory of turbulence generated jet noise, noise radiation from upstream sources and combination of noise, Technical Report AFAPL-TR-72-53, Lockheed Georgia Company, 1972.
[10] P. Mungur, G. Gladwell, Acoustic wave propagation in a sheared fluid contained in a duct, J. Sound Vib. 9 (1) (1969) 28–48.
[11] B.T. Chu, X. Kovasznay, Non-linear interactions in a viscous heat conducting compressible gas, J. Fluid Mech. 3 (5) (1958) 494–514.